Iron as a Bound Secondary Electron Donor in Modified Bacterial Reaction Centers†

L. Kálmán,‡,§ R. LoBrutto,‖ J. C. Williams,‡ and J. P. Allen*,‡

Department of Chemistry and Biochemistry and School of Life Sciences, Arizona State University, Tempe, Arizona 85287-1604

Received June 2, 2006; Revised Manuscript Received September 14, 2006

ABSTRACT: The binding and oxidation of ferrous iron were studied in wild-type reaction centers and in mutants that have been modified to be both highly oxidizing and able to bind manganese [Thielges et al. (2005) *Biochemistry 44*, 7389−7394]. After illumination of wild-type reaction centers, steady-state optical spectroscopy showed that the oxidized bacteriochlorophyll dimer, P^+, could oxidize iron but only as a second-order reaction at iron concentrations above 100 μM. In the modified reaction centers, P^+ was reduced by iron in the presence of sodium bicarbonate with dissociation constants of ∼1 μM for two mutants with different metal-binding sites. Transient optical spectroscopy showed that P^+ was rapidly reduced with first-order rates of 170 and 275 s^{-1} for the two mutants. The dependence of the amplitude of this rate on the iron concentration yielded a dissociation constant of ∼1 μM for both mutants, in agreement with the steady-state determination. The oxidation of bound iron by P^+ was confirmed by the observation of a light-induced EPR signal centered at *g* values of 2.2 and 4.3 and attributed to high-spin Fe^{3+}. Bicarbonate was required at pH 7 for low dissociation constants for both iron and manganese binding. The similarity between iron and manganese binding in these mutants provides insight into general properties of metal-binding sites in proteins.

In photosynthesis, the energy of light is converted into chemical energy through a chain of electron-transfer reactions involving a series of pigment−protein complexes embedded in the membrane (*1*, *2*). Purple bacteria perform anoxygenic photosynthesis with the primary photochemistry occurring in an integral membrane protein termed the reaction center. Light excites the bacteriochlorophyll dimer (P),[1] leading to the transfer of an electron from P to a series of acceptors, including the primary and secondary quinone acceptors, Q_A and Q_B, respectively. The light-induced formation of the oxidized bacteriochlorophyll dimer, P^+, is followed by reduction by secondary electron donors such as a water-soluble cytochrome c_2. Plants, algae, and cyanobacteria perform oxygenic photosynthesis with the primary photochemistry occurring in photosystems I and II. The primary electron donor of photosystem II, P680, is the most oxidizing agent in nature with an oxidation/reduction midpoint potential of ∼1.1 V (*3*). The high midpoint potential of P680 allows electron transfer through a tyrosine residue from the site of water oxidation, the manganese cluster.

The similarity of the core structures of the reaction center and photosystem II, despite differences in their function, provides an opportunity to mimic the water oxidation ability of photosystem II in the reaction center from *Rhodobacter sphaeroides* (*4*). Since P in the wild-type reaction center does not have a sufficient oxidation/reduction midpoint potential to oxidize tyrosine or manganese, the P/P^+ midpoint potential was increased to over 0.8 V as a result of a set of mutations near P (*5*). These modified reaction centers were able to oxidize tyrosine residues introduced at different locations in the reaction center (*6*). In combination with the mutations that produce highly oxidizing reaction centers, several mutations were introduced to provide possible manganese-binding ligands at a location in the reaction center that is comparable to that of the manganese cluster of photosystem II (*7*−*9*). Four combinations of different possible manganese ligands were introduced in the M1, M2, M3, and M4 mutants and compared to a control mutant that had a high midpoint potential but lacked the manganese-binding site. The M2 mutant was found to tightly bind manganese with a dissociation constant of 1 μM, while the M1 and M4 mutants bound manganese less tightly and the M3 mutant only bound manganese nonspecifically as was also found for the control mutant. The bound manganese was shown to be capable of serving as a secondary electron donor to the oxidized bacteriochlorophyll dimer, P^+. The dissociation constant for manganese binding increased sharply with decreasing pH due to the release of up to 1.5 protons upon manganese binding (*9*).

Several metalloproteins have been reported to be able to bind both manganese and iron. For example, the iron cofactor of ribonucleotide reductase can be replaced with manganese, and manganese has been observed at the iron-binding site of hemerythrin (*10*, *11*). The ability of some proteins to accommodate either manganese or iron led us to investigate the ability of the M1 and M2 mutants to bind and oxidize iron. Electron transfer between bound ferrous iron and P^+ was characterized by steady-state and transient optical

† This work was supported by Grant MCB 0131764 from the NSF.

* Corresponding author. Phone: 480-965-8241. Fax: 480-965-2747. E-mail: jallen@asu.edu.

‡ Department of Chemistry and Biochemistry, Arizona State University.

§ Permanent address: Department of Physics, Concordia University, Montreal, Quebec H4B 1R6, Canada.

‖ School of Life Sciences, Arizona State University.

[1] Abbreviations: P, bacteriochlorophyll dimer; Q_A, primary quinone; EPR, electron paramagnetic resonance.

10.1021/bi061104a CCC: $33.50
Published on Web 10/24/2006

spectroscopy as well as electron paramagnetic resonance (EPR) spectroscopy.

MATERIALS AND METHODS

Construction of the Mutants and Protein Isolation. Construction of the mutants in *R. sphaeroides* has been previously described (*7*, *12*). The highly oxidizing triple mutant contains the changes Leu L131 to His, Leu M160 to His, and Phe M197 to His that introduce three additional hydrogen bonds to P (*12*). In addition to these three mutations, the control mutant has an Arg M164 to Tyr substitution that is located near the metal-binding site. The metal-binding sites were constructed by introducing carboxylate residues near the dimer on the periplasmic side of the protein (*7*). The metal-binding mutants contain all four mutations found in the control mutant, and in addition M1 has the mutations Met M168 to Glu and Val M192 to Glu and M2 has the mutations Met M168 to Glu and Gly M288 to Asp. The strains were grown semiaerobically, and reaction centers were isolated and purified as described earlier, except that the detergent lauryl dimethylamine oxide was replaced with Triton X-100 in the ion-exchange chromatography step (*13*). After isolation, the samples were dialyzed for ~48 h against 0.03% Triton X-100 and 15 mM *N*-(2-hydroxyethyl)-piperazine-*N*′-2-ethanesulfonic acid, pH 7.

Optical Spectroscopy. Measurements were performed in the presence of excess terbutryne, unless otherwise stated, to block electron transfer from Q_A^- to Q_B. Ferrous iron sulfate solutions were prepared just prior to use. In most measurements, 15 mM sodium bicarbonate was added. Manganese chloride was added to the samples for the measurements of manganese binding.

A Cary 5 spectrophotometer (Varian) was used to measure the optical absorbance changes induced by continuous illumination. The light excitation was achieved using an Oriel tungsten lamp with an 860 nm interference filter. The illumination lasted no longer than 30 s, and the intensity was set to one-third of the intensity needed to saturate wild-type reaction centers. The spectra were recorded using a scanning rate of 900 nm/min. Flash-induced absorption transients were measured at 865 nm by a single beam spectrophotometer of local design (*14*). The reaction centers were excited at 532 nm with a 5 ns laser pulse using a ND:YAG laser (Continuum), and the kinetic traces were analyzed using exponential decomposition.

EPR Spectroscopy. Ferrous iron sulfate was added at a final concentration of 3 μM to a solution containing reaction centers at a concentration of 1 μM in the presence of 15 mM $NaHCO_3$, 0.03% Triton X-100, and 15 mM *N*-(2-hydroxyethyl)piperazine-*N*′-2-ethanesulfonic acid, pH 7. After 15−20 min incubation, the reaction centers were concentrated together with the bound iron in Centricon microconcentrators (Amicon) to a protein concentration of ~50 μM. After concentration, 20 mM $NaHCO_3$ and 300 μM terbutryne were added, followed by the addition of 50% glycerol as a cryoprotectant agent. The light-induced radicals were trapped by immersing the samples into liquid nitrogen immediately after illumination at room temperature as described elsewhere (*6*). Spectra were recorded at 120 K using a Bruker E580 X-band spectrometer equipped with an Oxford Model 900 EPL cryostat.

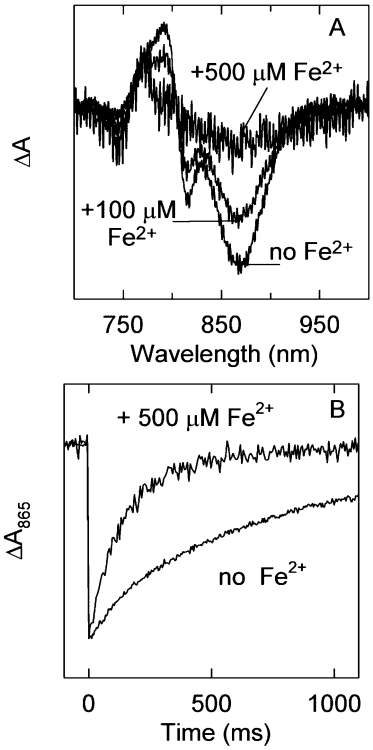

FIGURE 1: Iron oxidation in wild-type reaction centers measured using optical spectroscopy. (A) Changes in the light-minus-dark difference optical spectra in the presence of 0, 100, and 500 μM $FeSO_4$. Conditions: 1.5 μM reaction centers, 0.03% Triton X-100, 15 mM *N*-(2-hydroxyethyl)piperazine-*N*′-2-ethanesulfonic acid, pH 7, 15 mM $NaHCO_3$, and 100 μM terbutryne. (B) Kinetics of P^+ reduction measured by the change in absorption at 865 nm following a saturating laser flash. Without added iron, P^+ recovers via charge recombination from the reduced secondary quinone with a rate constant of 1.25 s^{-1}. In the presence of 500 μM $FeSO_4$ the observed recovery rate of P^+ increases to 6.6 s^{-1} due to reduction by the iron. Conditions as in panel A except without terbutryne.

Data Analysis. The dissociation constant of metal binding to the reaction center was determined using an analysis (*7*) based upon a previous investigation of metal binding in proteins (*15*). The fraction of reaction centers with bound metal, R_M, can be expressed in terms of the dissociation constant of metal binding, K_D, the concentration of added metal, [M], and the concentration of reaction centers, [RC], as

$$R_M = \frac{([M] + [RC] + K_D) - \sqrt{([M] + [RC] + K_D)^2 - 4[RC][M]}}{2[RC]} \quad (1)$$

In the steady-state measurements, $1 - R_M$ is given by the fraction of P^+, and in the transient measurements R_M is given by the fraction of the fast component. The protein concentration used is these measurements was ~1 μM, which places a lower limit of ~1 μM for the determined value of K_D.

RESULTS

Iron Oxidation by Wild-Type Reaction Centers. The ability of wild-type reaction centers to oxidize iron was measured using optical spectroscopy (Figure 1). In the absence of any secondary electron donor, light induces the formation of the state $P^+Q_A^-$ in the presence of terbutryne, as evidenced by

the absorption decrease near 865 nm due to P^+, an electrochromic shift of the bacteriochlorophyll monomer near 800 nm, and an absorption increase at 760 nm due to Q_A^-. At low iron concentrations, no changes of the spectrum were detected. In the presence of high concentrations of iron, the absorption decrease at 865 nm diminished as the iron concentration increased, with the spectrum at 500 μM iron being characteristic of Q_A^- alone. These optical changes indicate that Fe^{2+} serves as a secondary electron donor to P^+ but only at very high concentrations. The reaction was accompanied by the appearance of a brown precipitate, especially at high iron concentrations, due to the formation of an insoluble ferric iron compound, which impaired the optical quality of the samples. The high ferrous iron concentration needed to achieve substantial rereduction of P^+ indicates that the iron was not bound tightly.

The recovery of P^+ after a saturating laser flash excitation was measured at 865 nm. In the presence of terbutryne, no changes in the P^+ recovery rate of 10 s^{-1} due to $P^+Q_A^-$ charge recombination were observed with increasing iron concentration (data not shown), indicating that the iron oxidation rate is slower than the $P^+Q_A^-$ charge recombination rate in wild-type reaction centers. In the absence of iron and terbutryne, P^+ recovers with a 1.25 s^{-1} rate constant due to charge recombination from Q_B^-. At iron concentrations below 100 μM, the measured rate was unchanged. At higher concentrations, the observed rate increased with increasing iron concentrations up to a characteristic rate of 6.6 s^{-1} at 500 μM iron (Figure 1B). The highly oxidizing triple mutant, which also lacks a metal-binding site near P, showed a similar behavior (data not shown).

Iron Oxidation in the Mutant Reaction Centers. The binding of Fe^{2+} was measured in the M1, M2, and control mutants by determining the fraction of P^+ at different Fe^{2+} concentrations using steady-state optical spectroscopy (Figure 2). In the absence of iron, the light-induced spectra were consistent with formation of the state $P^+Q_A^-$. As iron was added in micromolar concentrations to the M1 and M2 mutants in the presence of bicarbonate at pH 7, the amount of P^+ decreased, with the spectral contributions of P^+ eliminated in the presence of 20 μM iron. The dependence of P^+ on the iron concentration yielded a dissociation constant of ~1 μM for the M1 and M2 mutants and 46 μM for the control mutant.

The recovery of P^+ after a saturating laser flash was measured for the mutants with electron transfer to the secondary quinone blocked by the addition of terbutryne (Figure 3). In the absence of iron, P^+ decays through charge recombination from Q_A^- with a rate constant of 23 s^{-1} in all of these mutants. This charge recombination rate is faster than the rate of 10 s^{-1} rate observed for wild-type reaction centers due to the increase in the P/P^+ midpoint potential compared to wild type (*16*). For the control mutant, the P^+ recovery did not change until the iron concentration was above 10 μM. Above 10 μM, the small changes could be fitted as arising from an additional decay component that increased from 65 to 95 s^{-1}, corresponding to a second-order rate constant of 2×10^5 M^{-1} s^{-1}. For the M1 and M2 mutants, the observed rate of the kinetic traces became distinctly biphasic after iron was added to the reaction centers, with the presence of a fast component in addition to the slow 23 s^{-1} component observed in the absence of iron. As the amount of iron increased, the amplitude of the fast component increased, and correspondingly the amplitude of the slow component decreased. The rates of both components were found to be independent of the iron concentration, showing that these were first-order electron-transfer reactions. The fast component was assigned to the oxidation of the bound iron by P^+ with rate constants of 275 and 170 s^{-1} for the M1 and M2 mutants, respectively. The dependence of the amplitude of the fast component on the iron concentration was used to determine the dissociation constant for binding in the M1 and M2 mutants (*7*). A tight binding was found between the reaction center and the iron with a dissociation constant of ~1 μM for both mutants, in agreement with the steady-state determination.

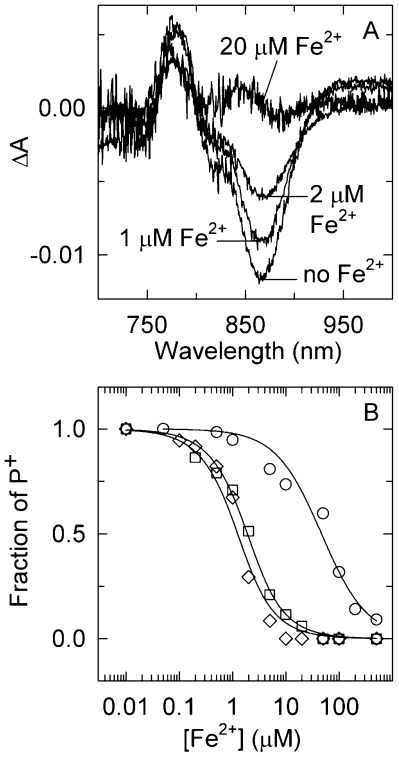

FIGURE 2: Iron binding and oxidation in mutant reaction centers studied by steady-state optical spectroscopy. (A) Changes in the light-minus-dark optical difference spectra in the presence of 0, 1, 2, and 20 μM $FeSO_4$ measured for the M1 mutant in the presence of bicarbonate at pH 7. The absorption band at 865 nm decreased with increasing ferrous iron concentration due to the oxidation of iron by P^+. (B) Fraction of P^+ at different iron concentrations for the M1 (squares), M2 (diamonds), and control (circles) mutants. The lines are fits of the data using eq 1 yielding dissociation constants of 1.3, 0.8, and 46 μM for the M1, M2, and control mutants, respectively. Conditions as in Figure 1A.

EPR Characterization of Iron Binding and Oxidation. Light-induced EPR spectra at 120 K were measured for the M1 mutant with and without added ferrous iron (Figure 4). In the absence of iron, the predominant signal is centered at the $g = 2.0$ region and arises from P^+ (*17*). The reduced semiquinone is not seen at 120 K as it is only measurable below 10 K due to broadening arising from the magnetic coupling of the quinone to the non-heme iron situated between the quinones. In the presence of added ferrous iron the light-induced spectrum is considerably different, with the signal at $g = 2.0$ significantly reduced and two new signals observed, a broad signal at $g = 2.2$ with a line width of 235 G and a relatively narrow signal at $g = 4.3$ with a line width

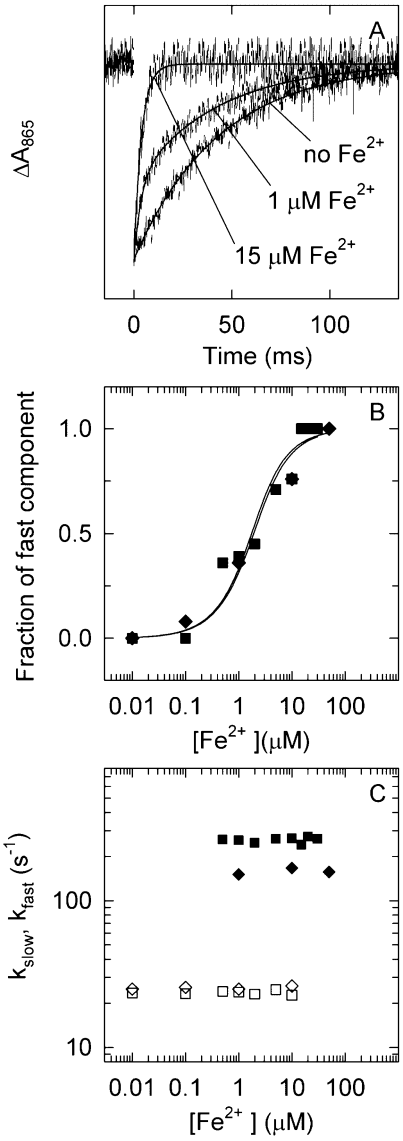

FIGURE 3: Kinetics of iron oxidation in mutant reaction centers measured by transient optical spectroscopy. (A) Representative kinetic traces of P^+ recovery after a laser flash excitation as measured by the absorption changes at 865 nm for iron concentrations of 0, 1, and 15 μM $FeSO_4$ for the M1 mutant. The traces were decomposed into two kinetic components with the slow component assigned to charge recombination from the reduced primary quinone and the fast component to the oxidation of the bound iron by P^+. (B) Fraction of the fast kinetic component as a function of the added iron concentration for the M1 (squares) and M2 (diamonds) mutants. The lines represent fits using eq 1, yielding dissociation constants of 1.2 and 1.1 μM for the M1 and M2 mutants, respectively. (C) Rate constants of the fast (closed symbols) and the slow (open symbols) kinetic components of the P^+ recovery as a function of the iron concentration for the M1 (squares) and M2 (diamonds) mutants. Conditions as in Figure 1A.

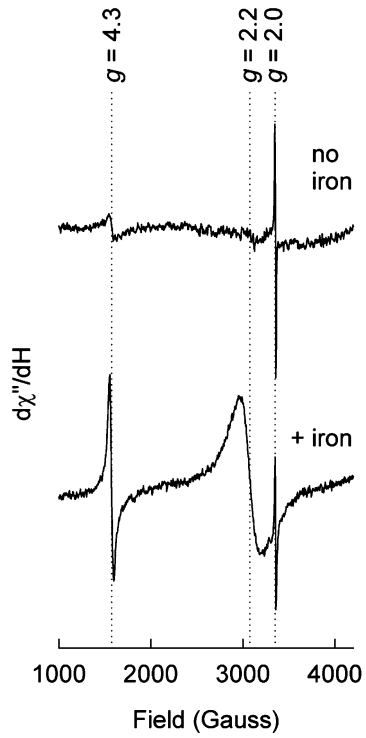

FIGURE 4: EPR spectra of reaction centers from the M1 mutant generated in the presence of light with and without iron. In the absence of iron, the dominant signal at a g value of 2.0 is due to P^+. In the presence of iron the P^+ signal decreases, and new signals emerge at g values of 2.2 and 4.3, indicating the presence of high-spin Fe^{3+}. The samples were illuminated at room temperature, and the light-induced signals were trapped by rapid freezing in liquid nitrogen for measurement at 120 K. Conditions: 100 kHz magnetic field modulation frequency, 0.4 mT modulation amplitude, 10 mW microwave power, 1.2 mT/s sweep rate, and 9.41 GHz microwave frequency.

of 44 G. The signals at $g = 2.2$ and 4.3 are assigned to the presence of high-spin Fe^{3+}. A signal was also observed at $g = 4.3$ for samples without added iron; this most likely arises from the binding of ambient iron that is oxidized after illumination. Although the $g = 4.3$ signal in principle can arise from both free and bound ferric irons, the presence of the intense signals only after illumination is a strong indication for oxidized iron being bound to the binding site. The precise identification of the electronic structure of the bound iron will require additional experiments, but the presence of the $g = 4.3$ signal indicates that the dominant species is a high-spin ferric iron with rhombic symmetry.

Effect of Bicarbonate on Metal Binding. The binding of iron to the M2 mutant was measured at pH 7 with and without 15 mM bicarbonate using steady-state optical spectroscopy as described above. The K_D value was ~1 μM in the presence of bicarbonate and was larger at 30 μM in the absence of bicarbonate (data not shown). For comparison, measurement of manganese binding to the M2 mutant resulted in K_D values of ~1 and 921 μM in the presence and absence of bicarbonate, respectively. Manganese binding has been shown to have a pronounced pH dependence for this K_D measured in the absence of bicarbonate (*9*). Due to the limited solubility of iron at higher pH values, the measurements involving iron could only be performed at pH 7. However, measurements of manganese binding performed at pH 9 yielded a K_D value of ~1 μM with and without bicarbonate.

DISCUSSION

Both the binding of manganese and the oxidation of bound manganese by P^+ generated in the light were previously demonstrated in a series of modified bacterial reaction centers in which binding sites were introduced by addition of carboxylate residues near the surface of the protein (*7*). In this report, two of these mutant reaction centers, from the

M1 and M2 strains, have been shown to also be able to bind iron with a dissociation constant of ~1 μM, determined using two independent measurements. The bound iron serves as a secondary electron donor, reducing P^+ in a first-order process. The oxidation of the iron was confirmed by EPR measurements that showed the presence of signals from a high-spin Fe^{3+}. The features of the iron binding enhance our understanding of the metal-binding capabilities of these mutants as discussed below.

Three types of reaction centers without binding sites were examined, the wild type, a highly oxidizing triple mutant with mutations near P that raise the P/P^+ midpoint potential, and a control mutant that contains the mutations in the triple mutant plus a change introducing a tyrosine residue near the binding site. Neither the wild type nor the triple mutant showed iron oxidation except at very high iron concentrations, indicating that the binding was nonspecific. Similarly, only very weak binding of manganese was observed for reaction centers when no metal-binding site was present (*8*). In steady-state measurements of iron binding, the control mutant showed spectral changes at relatively lower iron concentrations of 40 μM, yielding a dissociation constant of 46 μM compared to 172 and 160 μM for wild type and the triple mutant, respectively. In kinetic measurements at an iron concentration of 500 μM, the second-order rate of iron oxidation based upon the observed rates of P^+ decay was approximately 15 times faster for the control mutant than for the wild type and triple mutant. The Arg M164 to Tyr mutation found in the control, M1, and M2 mutants but not the triple mutant has been shown previously to be required for the strong manganese binding in the M2 mutant (*9*), and it is likely that this mutation enables the participation of Glu M173 in the metal-binding site, as Arg M164 and Glu M173 form a salt bridge in the wild type. However, the M164 Arg to Tyr mutation alone does not provide a tight binding site for manganese or iron.

The amino acid residues Tyr, Asp, Glu, and His are commonly found as ligands for non-heme iron cofactors and dinuclear iron cofactors in proteins such as transferrin and ribonucleotide reductase (*18*, *19*). In the M2 mutant, manganese has been shown to bind to two introduced carboxylate groups, Glu M168 and Asp M288, as well as Glu M173, His M193, and a bound water molecule with Tyr M164 being also near the binding site (*7*). The M1 and M2 mutants both bound iron, indicating that the carboxylate residues introduced in the M1 and M2 mutants are required for iron binding. On the basis of the structure of manganese bound to the M2 mutant, iron likely binds to Glu M168 and His 193 in both the M1 and M2 mutants. The nearby amino acid residues, such as Tyr M164 and Glu M173, also may participate in the iron binding as they do in manganese binding in the M2 mutant. The binding sites for the M1 and M2 mutants differ in that the M1 mutant has the alteration of Val M192 to Glu and M2 has Gly M288 changed to Asp. These differences between the M1 and M2 mutants appear to play only a minor role in determining iron binding in the presence of bicarbonate.

The first-order kinetics of iron oxidation confirmed that the iron was bound to the mutants. Despite having the same dissociation constant of ~1 μM, the rate of iron oxidation was appreciably faster in the M1 mutant than in the M2 mutant, with rate constants of 275 and 170 s^{-1}, respectively. This difference in the rate of iron oxidation could reflect a difference between the two mutants in the free energy difference, the reorganization energy, or the coupling of the $Fe^{2+}P^+Q_A^-$ to $Fe^{3+}PQ_A^-$ electron-transfer reaction. The free energy difference is dependent on the difference between the P/P^+ and Fe^{2+}/Fe^{3+} midpoint potentials. The P/P^+ midpoint potential in the M1 and M2 mutants is most probably very similar, as indicated by the negligible differences in the observed rate constants for $P^+Q_A^-$ charge recombination. However, a difference in the iron coordination in the M1 and M2 mutants could easily alter the Fe^{2+}/Fe^{3+} midpoint potential, the precise distance between the iron and P, or the reorganization energy associated with the iron oxidation, with resulting changes in the rate.

Bicarbonate was shown to play a critical role in facilitating metal binding at pH 7. The effect of bicarbonate at different pH values is most clearly seen in the binding of manganese. In the absence of bicarbonate, the K_D for manganese binding shows a strong pH dependence, with a large increase in the dissociation constant at lower pH (*9*). Modeling this behavior indicates that below pH 8.5 manganese binding requires the release of up to two protons, while above pH 8.5 the coordinating ligands are deprotonated prior to binding, and the manganese binding becomes pH independent. In the presence of bicarbonate, the binding at pH 9 matches that observed without bicarbonate, while at pH 7 the K_D value does not change relative to the value at pH 9, in contrast to the increase observed in the absence of bicarbonate. Thus, bicarbonate probably facilitates manganese binding by removing the requirement of proton release upon metal binding between pH 7 and pH 8.5. The binding of iron to the mutants could only be measured at pH 7 due to the limited solubility of the ferrous iron sulfate solutions at higher pH values. The lower dissociation constant observed for iron binding at pH 7 in the presence of bicarbonate compared to binding in the absence of bicarbonate implies that bicarbonate facilitates iron binding in a similar manner.

In non-heme proteins, synergistic anions, such as bicarbonate, can coordinate bound metal ions either as bidentate or monodentate ligands depending on the stereochemical requirements of the metal ion and the nature of the anion-binding crevice (*18*, *20*). In these proteins, the syngeristic anion is bound through hydrogen bonds and electrostatic interactions, and sometimes a close interaction with an arginine residue. Bicarbonate probably also binds to the reaction center at the metal-binding site. The metal-binding site in the M1 and M2 mutants would provide several possible hydrogen-bonding interactions for bicarbonate binding. Binding of bicarbonate would be consistent with manganese binding at pH 9 having different dissociation constants in the two mutants in the absence of bicarbonate but the same dissociation constant in the presence of bicarbonate. If bicarbonate only facilitated binding but did not actually bind, then it would be expected that the dissociation constants would be different for the two mutants. For both iron and manganese at pH 7 with bicarbonate, the binding was similar in the M1 and M2 mutants, indicating that the bicarbonate provides some of the ligands.

The ability of iron to be oxidized by the reaction centers has implications for the evolutionary development of photosynthetic systems. On the basis of these results, ferrous iron can function as a secondary electron donor to wild-type

reaction centers from *R. sphaeroides*. The physiological significance of this is suggested by the ability of some strains of purple non-sulfur bacteria to oxidize ferrous iron to ferric iron during photosynthetic growth (*21*). Direct biological oxidation of ferrous iron by primitive anoxygenic photosynthetic organisms is one of the scenarios to explain the origin of banded iron formations that were created before the oxygenic atmosphere emerged on Earth as a result of the evolutionary development of primitive cyanobacteria (*22*). In a speculative pathway to oxygenic photosynthesis, once the P/P^+ midpoint potential increased, primitive reaction centers with a metal-binding site could have used manganese as an efficient secondary electron donor until they gained the capacity for water oxidation with the advent of the manganese cluster (*4*, *23*).

ACKNOWLEDGMENT

We thank Lisa Lauman for the growth of the bacterial cultures.

REFERENCES

1. Blankenship, R. E., Madigan, M. T., and Bauer, C. E., Eds. (1995) *Anoxygenic Photosynthetic Bacteria*, Kluwer Academic Publishers, Dordrecht, The Netherlands.
2. Ort, D. R., and Yocum, C. F., Eds. (1996) *Oxygenic Photosynthesis: The Light Reactions*, Kluwer Academic Publishers, Dordrecht, The Netherlands.
3. Wydrzynski, T., and Satoh, K., Eds. (2005) *Photosystem II: The Light-Driven Water:Plastoquinone Oxidoreductase*, Springer Publishers, Dordrecht, The Netherlands.
4. Kálmán, L., Williams, J. C., and Allen, J. P. (2005) Mimicking the properties of photosystem II in bacterial reaction centers, in *Photosystem II: The Light-Driven Water:Plastoquinone Oxidoreductase* (Wydrzynski, T., and Satoh, K., Eds.) pp 715−727, Springer Publishers, Dordrecht, The Netherlands.
5. Kálmán, L., LoBrutto, R., Allen, J. P., and Williams, J. C. (1999) Modified reaction centres oxidize tyrosine in reactions that mirror photosystem II, *Nature 402*, 696−699.
6. Narváez, A. J., LoBrutto, R., Allen, J. P., and Williams, J. C. (2004) Trapped tyrosyl radical populations in modified reaction centers from *Rhodobacter sphaeroides*, *Biochemistry 43*, 14379−14384.
7. Thielges, M., Uyeda, G., Cámara-Artigas, A., Kálmán, L., Williams, J. C., and Allen, J. P. (2005) Design of a redox-linked active metal site: Manganese bound to bacterial reaction centers at a site resembling that of photosystem II, *Biochemistry 44*, 7389−7394.
8. Kálmán, L., LoBrutto, R., Allen, J. P., and Williams, J. C. (2003) Manganese oxidation by modified reaction centers from *Rhodobacter sphaeroides*, *Biochemistry 42*, 11016−11022.
9. Kálmán, L., Thielges, M. C., Williams, J. C., and Allen, J. P. (2005) Proton release due to manganese binding and oxidation in modified bacterial reaction centers, *Biochemistry 44*, 13266−13273.
10. Atta, M., Nordlund, P., Åberg, A., Eklund, H., and Fontecave, M. (1992) Substitution of manganese for iron in ribonucleotide reductase from *Escherichia coli*, *J. Biol. Chem. 267*, 20682−20688.
11. Zhang, J. H., and Kurtz, D. M. (1992) Metal substitutions at the diiron sites of hemerythrin and myohemerythrin: Contributions of divalent metals to stability of a four-helix bundle protein, *Proc. Natl. Acad. Sci. U.S.A. 89*, 7065−7069.
12. Lin, X., Murchison, H. A., Nagarajan, V., Parson, W. W., Allen, J. P., and Williams, J. C. (1994) Specific alteration of the oxidation potential of the electron donor in reaction centers from *Rhodobacter sphaeroides*, *Proc. Natl. Acad. Sci. U.S.A. 91*, 10265−10269.
13. Williams, J. C., Alden, R. G., Murchison, H. A., Peloquin, J. M., Woodbury, N. W., and Allen, J. P. (1992) Effects of mutations near the bacteriochlorophylls in reaction centers from *Rhodobacter sphaeroides*, *Biochemistry 31*, 11029−11037.
14. Kleinherenbrink, F. A., Chiou, H. C., LoBrutto, R., and Blankenship, R. E. (1994) Spectroscopic evidence for the presence of an iron-sulfur center similar to Fx of photosystem I in *Heliobacillus mobilis*, *Photosynth. Res. 41*, 115−123.
15. Gerencsér, L., and Maróti, P. (2001) Retardation of proton transfer caused by binding of the transition metal ion to the bacterial reaction center is due to pK_a shifts of key protonatable residues, *Biochemistry 40*, 1850−1860.
16. Allen, J. P., Williams, J. C., Graige, M. S., Paddock, M. L., Labahn, A., Feher, G., and Okamura, M. Y. (1998) Free energy dependence of the direct charge recombination from the primary and secondary quinones in reaction centers from *Rhodobacter sphaeroides*, *Photosynth. Res. 55*, 227−233.
17. Feher, G., Allen, J. P., Okamura, M. Y., and Rees, D. C. (1989) Structure and function of bacterial photosynthetic reaction centers, *Nature 339*, 111−116.
18. Sun, H., Li, H., and Sadler, P. J. (1999) Transferrin as a metal ion mediator, *Chem. Rev. 99*, 2817−2842.
19. Stubbe, J., and van der Donk, W. A. (1998) Protein radicals in enzyme catalysis, *Chem. Rev. 98*, 705−762.
20. Shongwe, M. S., Smith, R., Marques, H. M., and van Wyk, J. A. (2004) Synergistic anion-directed coordination of ferric and cupric ions to bovine serum transferrin—an inorganic perspective, *J. Inorg. Biochem. 98*, 199−208.
21. Widdel, F., Schnell, S., Heising, S., Ehrenreich, A., Assmus, B., and Schink, B. (1993) Ferrous iron oxidation by anoxygenic phototrophic bacteria, *Nature 362*, 834−836.
22. Dismukes, G. C., and Blankenship, R. E. (2005) The origin and evolution of photosynthetic oxygen production, in *Photosystem II: The Light-Driven Water:Plastoquinone Oxidoreductase* (Wydrzynski, T., and Satoh, K., Eds.) pp 683−695, Springer Publishers, Dordrecht, The Netherlands.
23. Blankenship, R. E., and Hartman, H. (1998) The origin and evolution of oxygenic photosynthesis, *Trends Biol. Sci. 23*, 94−97.

BI061104A